View metadata, citation and similar papers at core.ac.uk

brought to you by CORE

provided by Elsevier - Publisher Connector

Available online at www.sciencedirect.com

ScienceDirect

Procedia Materials Science 3 (2014) 104 – 109

Procedia Materials Science

www.elsevier.com/locate/procedia

20th European Conference on Fracture (ECF20)

Cracks pattern formation and spalling in functionalized thin films

Leguillon D.*, Haddad O., Adamowska M., Da Costa P.

Institut Jean Le Rond d'Alembert, CNRS UMR7190, Sorbonne universités, UPMC université Paris 6,4 place Jussieu, Paris 75005, France

Abstract

Functionalized thin films of ceramic material are used in catalytic converters as a catalyst support. A degradation of the catalytic performances can be caused by thermal and chemical effects leading to the formation of cracks and the detachment of fragments. Understanding the formation of the lattice of cracks and the spalling is challenging in fracture mechanics. The need for two conditions for predicting crack nucleation, one involving energy and the other stresses, is shown. The stress condition defines a threshold below which the pattern formation is inhibited. As long as it is not reached, the energy accumulates. Then, at onset, depending on the strength and toughness of the material, the amount of energy can be sufficiently large to give rise to a more or less dense lattice of cracks. Following initiation, the newly created small fragments tend to separate from it by debonding.

© 2014 Published by Elsevier Ltd. Open access under CC BY-NC-ND license.

Selection and peer-review under responsibility of the Norwegian University of Science and Technology (NTNU), Department of Structural Engineering

Keywords: Thin films, brittle materials, ageing, cracks pattern.

1. Introduction – The catalytic converter and the mechanical model

Functionalized thin films of ceramic material are increasingly used in the industry. For example, in automotive catalytic converters, in response to new environmental regulations, a honeycomb structure is covered by a thin layer of γ-Alumina as a catalyst support (Fig. 2). The degradation of the catalytic performances with time of stream can be caused by thermal and chemical effects leading to the formation of cracks and the detachment of fragments (Fig. 1).

* Corresponding author. Tel.: +33 144 275 322; fax: +33 144 275 259.
E-mail address: dominique.leguillon@upmc.fr

2211-8128 © 2014 Published by Elsevier Ltd. Open access under CC BY-NC-ND license.

Selection and peer-review under responsibility of the Norwegian University of Science and Technology (NTNU), Department of Structural Engineering
doi:10.1016/j.mspro.2014.06.020

Understanding the formation of the lattice of cracks (see e.g. Jenkins, 2009; Bahr et al., 2010; Shao et al., 2010; Jiang et al. 2012; Maurini et al., 2013; Sicsic et al., 2014) and the spalling is still challenging in fracture mechanics.

When analyzing the nucleation of cracks, the need for two conditions, one involving energy and the other one stresses, has recently been shown (Leguillon, 2002). The stress condition defines a threshold below which the pattern formation is inhibited. As long as it is not reached, the energy accumulates. Then, at onset, depending on the strength and toughness of the material, the amount of energy can be sufficiently large to give rise to a more or less dense lattice of cracks (Leguillon, 2013).

Following the formation of the cracks pattern, when the transverse crack tips are close to the support, the newly created small fragments tend to separate from it by debonding.

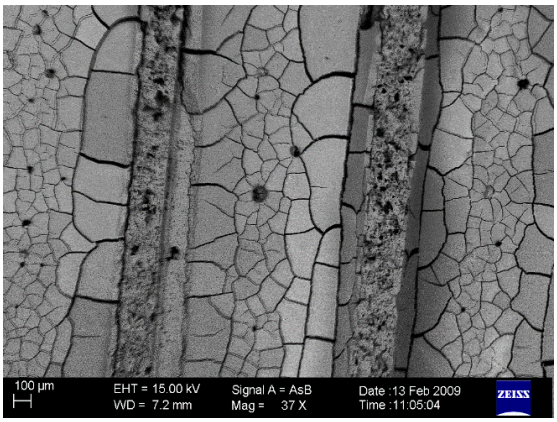

Figure 1. View of a section of the catalytic converter after artificial ageing.

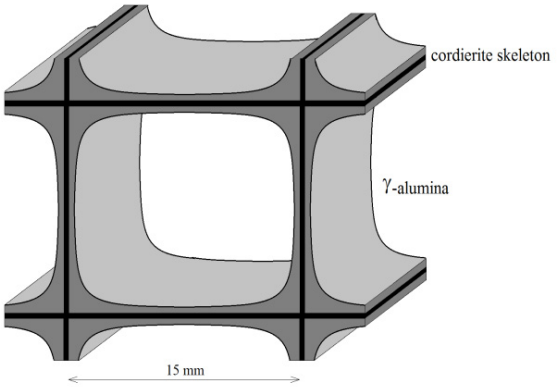

Fig. 2. The honey comb structure of the catalytic converter.

The skeleton of the honeycomb structure (Fig. 2) is made of a refractive material (cordierite) assumed as rigid and insensitive to thermal and chemical effects. The catalyst support is in γ-alumina: E= 250 GPa, Young's modulus, ν= 0.2, Poisson's ratio, α=6 10^{-6} K^{-1}, thermal expansion coefficient (Gallas and Piermarini, 1994). The thickness is less than 0.1 mm but not constant and is a parameter of this analysis. The structure is subjected to a thermal cycle intended to artificially simulate aging.

The constitutive law of the functionalized layer is expressed as a stress/strain relationship

$$\underline{\underline{\sigma}} = \mathbf{C} : \left(\underline{\underline{\varepsilon}}(\underline{U}) - \underline{\underline{\varepsilon}}^{\mathrm{an}} \right)$$

Where $\underline{U}$ denotes the displacement field, $\underline{\underline{\sigma}}$ the stress field, $\mathbf{C}$ the elastic tensor (relying on the Young modulus E and the Poisson ratio ν) and $\underline{\underline{\varepsilon}}(\underline{U})$ the linearized strain tensor (i.e. the symmetric part of the gradient of $\underline{U}$). The non-elastic part of the strain $\underline{\underline{\varepsilon}}^{\mathrm{an}}$ is assumed to be a pure dilatation

$$\varepsilon_{ij}^{\mathrm{an}} = \varepsilon^{\mathrm{an}} \delta_{ij}$$

Where δ_{ij} holds for the Kronecker symbol and $\varepsilon^{\mathrm{an}}$ is a constant. This non-elastic part of the total strain can be due to a thermal change (thermo-elasticity)

$$\varepsilon^{\mathrm{an}} = \alpha \Delta\theta$$

With α the thermal expansion coefficient and $\Delta\theta$ the temperature change. It can also be due to a phase change triggering a shrinkage. Then, it depends both on the temperature and the curing duration, in the present case it can be

due to both mechanisms. Nevertheless, in the following, by lack of data on the effects of phase change (this study is still in progress), only thermal expansion will be taken into account. It is assumed that at the initial temperature there is no residual stress and then the structure is cooled down i.e. $\Delta\theta \le 0$ and according to the experiments (Adamowska et al., 2013) $|\Delta\theta| \le$ 500 K (maximum thermal deformation $|\varepsilon^{an}| \le 3^{o}/_{oo}$).
However, if the solution prior to fracture is known (2)-(3), the energy stored in the fragments after fracture must be computed by FE. Any change δW^{P} in the potential energy of a fragment with length l resumes to a change of the strain energy

$$-\delta W^{P}(l) = \delta\left(\frac{1}{2}\int_0^l\int_0^e \mathbf{C} : \underline{\underline{\varepsilon}}(\underline{U}) : \underline{\underline{\varepsilon}}(\underline{U})\mathrm{d}x_1\mathrm{d}x_2\right) = \delta W(l) \text{ with } W(l) = \frac{1}{2}\int_0^l\int_0^e \mathbf{C} : \underline{\underline{\varepsilon}}(\underline{U}) : \underline{\underline{\varepsilon}}(\underline{U})\mathrm{d}x_1\mathrm{d}x_2$$

After a fragmentation in n parts with length $l=L/n$ (W^0 is the energy prior to fracture)

$$-\delta W^{P} = nW(l) - W^{0} \tag{1}$$

2. The 2D model for cracks pattern formation

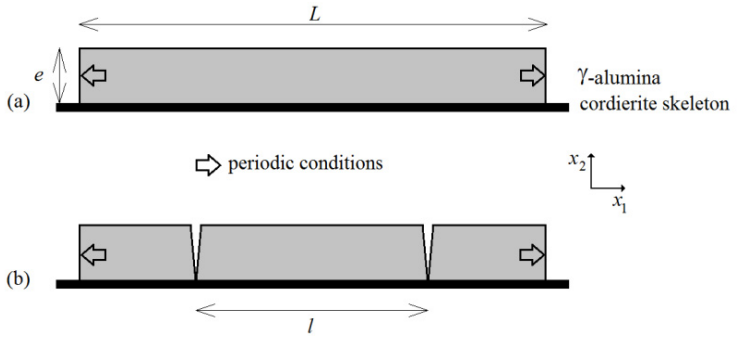

Fig. 3. The Plane strain 2D model. (a) Prior to fragmentation, (b) after fragmentation in two equal parts with length l .

The problem is expressed here in plane elasticity (plane strain), in a plane perpendicular to the channels of the converter (Fig. 2). The simplified geometry (Fig. 3) is made of a rectilinear alumina layer with a constant thickness e. Periodic conditions are used at the two ends in order to avoid edge effects that do not exist in the original geometry (Fig. 3(b)). Moreover we assumed that the plate is perfectly clamped on the rigid support. Prior to any fracture, the solution is

$$\sigma_{11} = -\frac{E}{(1+\nu)(1-\nu)}\varepsilon^{an};\ \sigma_{12} = \sigma_{22} = 0 \tag{2}$$

It may be noted in passing that the plane strain assumption implies $\sigma_{33} = \nu\sigma_{11} < \sigma_{11}$. Numerical computations using a standard FE code allows identifying the function $W(l)$ in two parts, and finally from (1) it comes

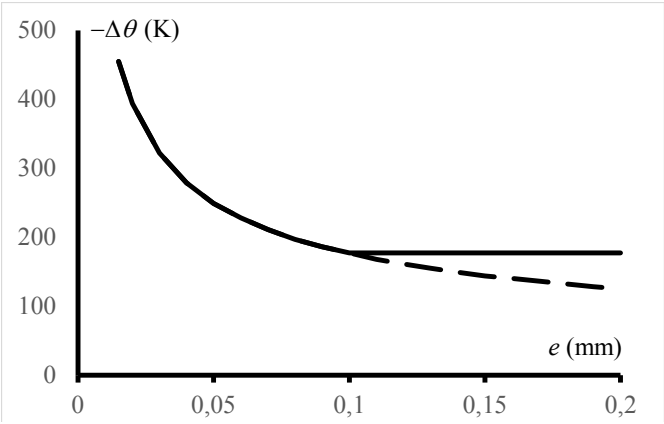

Fig. 4. The cooling $-\Delta\theta$ triggering the cracks pattern formation vs. the thickness e of the alumina layer.

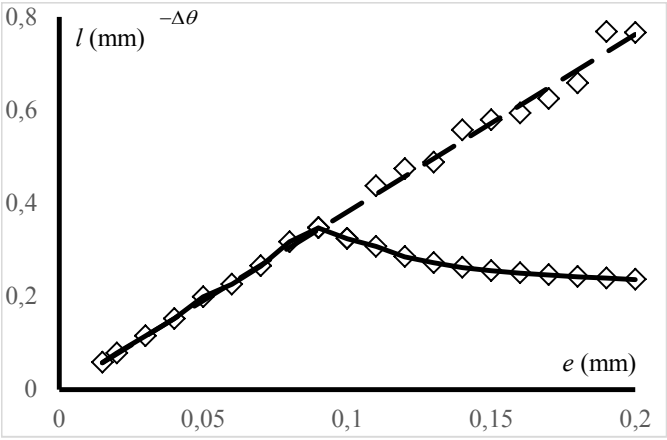

Fig. 5. The fragment size l vs the thickness e of the alumina layer.

- $l/e > 4 \quad -\delta W^{\mathrm{P}} \simeq n a_2 e^2 \varepsilon^{\mathrm{an}\,2}$
- $l/e \le 4 \quad -\delta W^{\mathrm{P}} \simeq L(a_1 l - 4a_1 e + \frac{1}{4e} a_2 e^2)\varepsilon^{\mathrm{an}\,2}$

with $a_1 = -0.06$ and $a_2 = 1.08$

These expressions must be compared to the energy $n \times (G_c e)$ per unit width (plane elasticity) consumed to create n cracks of length e (i.e. n pieces). The toughness G_c of γ-alumina is taken 0.03 MPa mm, indeed this value is unknown and derived from that of α-alumina 0.04 MPa mm, knowing that γ-alumina is more porous.

Then fragmentation occurs if

- $l/e > 4 \quad -\delta W^{\mathrm{P}} \ge n(G_c e) \;\Rightarrow\; e \ge \dfrac{G_c}{a_2 \varepsilon^{\mathrm{an}\,2}}$
- $l/e \le 4 \quad -\delta W^{\mathrm{P}} \ge n(G_c e)$

$$\Rightarrow l\left(a_1 \frac{l}{e} - 4a_1 + \frac{1}{4} a_2\right)\varepsilon^{\mathrm{an}\,2} \ge G_c$$

As expected from the periodic conditions these expressions are independent of L. The first condition leads to an unrealistic inequality and must be discarded. The second inequality is solved for the smaller $|\Delta\theta|$ (involved in $\underline{\underline{\varepsilon}}^{\mathrm{an}}$) giving an admissible fragment length l.

In addition, according to the coupled criterion, one has to check the stress condition, the tensile stress σ_{11} must be larger than the tensile strength $\sigma_c = 280$ MPa (this value is selected as above) all along the presupposed crack path, then using (2) $\sigma_{11} \ge \sigma_c \;\Rightarrow\; |\Delta\theta| \ge 180$ K. It means that solutions $|\Delta\theta|$ of (14) smaller than 180 K are not acceptable solutions. No fragmentation can occur below this cooling amplitude, whatever the thickness is.

Results are shown in Fig. 4. Obviously, for layer thicknesses lower than 0.1 mm, the cracks pattern formation is governed by the energy condition while one has to switch to the stress condition for thicker layers. Thus thin layers are more resistant to fragmentation. Another consequence is that, when governed by the energy condition, the fragment size increases linearly with the thickness (roughly l=4e) whereas this size decreases when governed by the stress conditions (Fig. 5). Roughly for $e \le$ 0.1 mm, thinner the layer, smaller the fragments; this is in agreement with observations made in Fig. 1 where the thickness in the central part of the channel is smaller than that of the lateral ones.

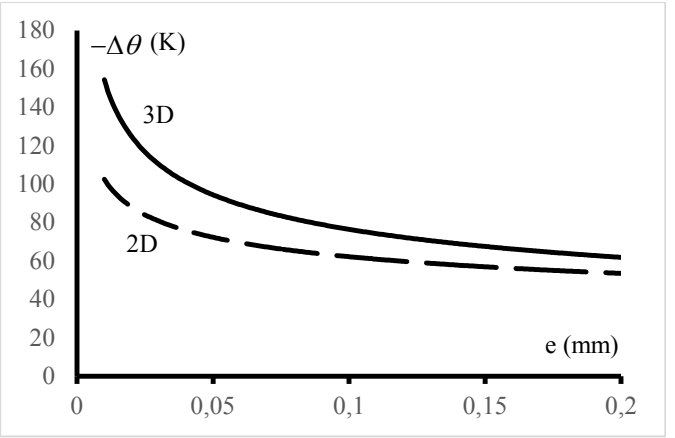

Fig. 6. The temperature drop triggering the initiation of debonding. The 2D model (dashed line), debonding from the bottom edge. The 3D model (solid line), debonding from the corner.

Once the cracks pattern is formed, there is a singularity and thus a stress concentration along the bottom edges of the fragments. The singularity is characterized by an exponent $\lambda_{2D} = 0.781$. The 2D coupled criterion in its explicit form (Leguillon, 2002) can be used to determine the temperature change triggering the pulling-out initiation. Again, thicker the layer, weaker the adhesion, i.e. smaller the temperature change triggering delamination. The temperature change evolves like $1/e^{1-\lambda_{2D}}$ (Fig. 6). Using the fracture properties of the γ-alumina, although those of the interface alumina/support should be selected but they are in general unknown and difficult to determine, shows that the temperature changes involved in this mechanism are by far lower than that triggering the cracks pattern, the fragmentation evolves immediately in a partial debonding. Moreover, it observed that the stress intensity factor at the tip of the interface crack that grows decreases to 0 with the crack length. Thus the debonding cannot lead to a complete pull-out of the fragment for a reasonable range of temperature change, it can only be achieved under mechanical actions like vibrations of the vehicle for instance.

3. The 3D model

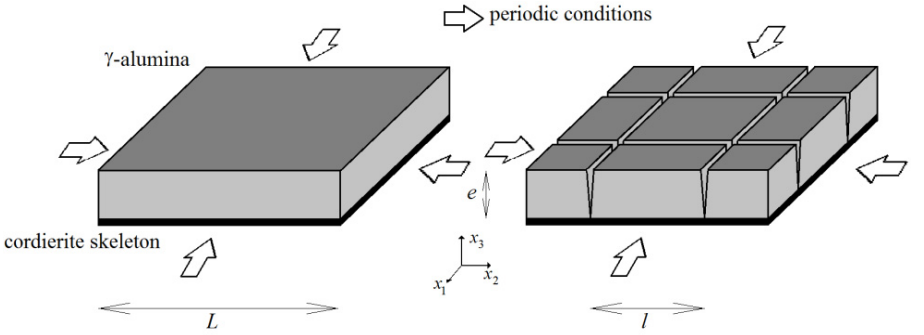

Fig. 7. The 3D model prior to cracks pattern formation and after a fragmentation into 4 square parts $l \times l$ (keep in mind the periodic conditions).

The simplified geometry is shown in Fig. 7 and boundary conditions are similar to the 2D case (clamped below and periodic around). One difference lies in the 3D stress field prior to failure (to be compared to (2))

$$\sigma_{11} = \sigma_{22} = -\frac{E}{1-\nu}\varepsilon^{an};\ \sigma_{12} = \sigma_{13} = \sigma_{23} = \sigma_{33} = 0 \tag{3}$$

Leading to a quite smaller threshold between the energy governed regime and the stress governed one: $|\Delta\theta| \geq 150$ K instead of 180 K.

Otherwise, all trends already observed in 2D are recovered in 3D (see Figs. 4 and 5). The aspect ratio of the fragments is still roughly 4, i.e. l=4e, above the threshold and diminishes below. The role of the thickness is unchanged, thicker the layer and weaker it is.

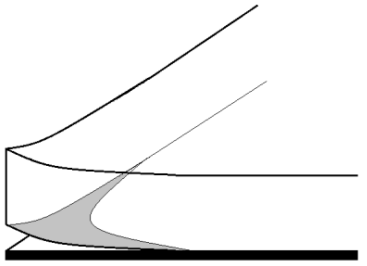

Fig. 8. A debonding starting from the corner.

The main difference lies in the description of the initiation of the debonding mechanism (Veluri and Jensen, 2013). The corner singularity is stronger $\lambda_{3D} = 0.695$ which might suggest that delamination starts from the corners rather than along the edges (Fig. 8). The 3D form of the coupled criterion is similar to the 2D one (Leguillon, 2014)

$$K^{xD} \geq K_c^{xD} = (G_c / A_{xD})^{1-\lambda_{xD}} \sigma_c^{xD\,2\lambda_{xD}-1} \text{ for xD=2D or 3D} \quad (4)$$

Where K^{xD} is the generalized stress intensity factor of the singularity, K_c^{xD} its critical value, and A_{xD} denotes a scaling coefficient that differs from 2D to 3D as well as the singular exponent λ_{xD}. There is a linear relationship between K^{xD} and ε^{an} or $\Delta\theta$ and the 3D criterion (4) allows expressing the critical temperature drop leading to a debonding starting from the corner. Its application contradicts the first conclusion based on the singular exponent, for thin layers the 2D condition for debonding prevails over the 3D one (Fig. 6). This trend is reversed only for high thicknesses (roughly $e \geq 1$ mm). In agreement with this conclusion, debonding is not visible in Fig. 1 but other images clearly show a full debonding all along the bottom edges of the fragments.

4. Conclusion

This study is still ongoing, now results remain rather qualitative either in terms of fragments size or critical temperature drop. There are two regimes for cracks pattern formation, one is governed by the energy condition and the other by the stress condition. Only larger thicknesses are affected by the stress condition. Once the fragments are formed there is a risk of detachment detrimental to the catalyst efficiency. The analysis of this mechanism can be conducted in two different ways depending on whether the debonding starts from the bottom edges or from the corners. In the first case, a 2D model is sufficient whereas a 3D Model is required in the other. Numerical tests on thin layers (< 1 mm) show that the 2D model should be preferred in the present case meaning that debonding occurs first along the bottom edges. This is sometimes reported in the study of the pulling-out of electron chips.

References

Adamowska M., Haddad O., Leguillon D., da Costa P., 2013. On the comprehension of mechanical, thermal and chemical evolution of exhaust gases after treatment catalysts, International Conference on Processing and Manufacturing of Advanced Materials, THERMEC'2013, Las Vegas, USA, December 2-6, 2013.

Bahr H.A., Weiss H.J., Bahr U., Hofmann M., Fisher G., Lampenscherf S., Balke H., 2010. Scaling behavior of thermal shock crack patterns and tunneling cracks driven by cooling or drying, J. Mech. Phys. Solids 58, 1411-1421.

Jenkins D.R., 2009. Determination of crack spacing and penetration due to shrinkage of a solidifying layer, Int. J. Solids Structures 46, 1078-1084.

Jiang C.P., Wu X.F., Li J., Song F., Shao Y.F., Xu X.H., Yan P., 2012. A study of the mechanism of formation and numerical simulations of crack patterns in ceramics subjected to thermal shock, Acta Mater. 60, 4540-4550.

Leguillon D., 2002. Stress or toughness, a criterion for crack onset at a notch. Eur. J. Mech. A/Solids 21, 61-72.

Leguillon D., 2013. A simple model of thermal crack pattern formation using the coupled criterion. C. R. Mécanique, 341, 538-546.

Leguillon D., 2014. An attempt to extend the 2D coupled criterion for crack nucleation in brittle materials to the 3D case, submitted.

Maurini C., Bourdin B., Gauthier G., Lazarus V., 2013. Crack patterns obtained by unidirectional drying of a colloidal suspension in a capillary tube : experiments and numerical simulations using a two-dimensional approach, InT. J. Fract. 184, 75-91.

Shao Y., Xu X., Meng S., Bai G., Jiang C., Song F., 2010. Crack patterns in ceramic plates after quenching, J. Am. Ceram. Soc. 93(10), 3006-3008.

Sicsic P., Marigo J.J., Maurini C., 2014. Initiation of a periodic array of cracks in the thermal shock problem: a gradient damage modeling, J. Mech. Phys. Solids 63, 256-284.

Veluri B., Jensen H.M., 2013. Steady-state propagation of interface corner crack, Int. J. Solids Structures 50, 1613-1620.